Electrical Power and Energy Systems 172 (2025) 111113

Contents lists available at ScienceDirect

International Journal of Electrical Power and Energy Systems

journal homepage: www.elsevier.com/locate/ijepes

Smart seismic rocking motion control of fluid tanks using semi-active model-based and data-driven adaptive control

Seyed Ehsan Aghakouchaki Hosseini *, Sherif Beskhyroun

Department of Built Environment Engineering, School of Future Environments, Faculty of Design and Creative Technologies, Auckland University of Technology (AUT), 1010 Auckland, New Zealand

ARTICLE INFO

Keywords:
Fluid storage tanks
Data-driven adaptive control
Smart rocking isolation
MR damper

ABSTRACT

Various mechanisms have been investigated in the literature for seismic protection of fluid tanks. These structures play a pivotal role in the integrity, reliability, and safety of strategic industries. Any damage to fluid tanks can jeopardise these industries and the environment. In this research, a Smart Vertical Isolation System using magnetorheological dampers for rocking isolation of legged rigid cylindrical fluid tanks under base excitations has been proposed and investigated. First, dynamic equations of motion for the rocking rigid fluid tank are developed. Different semi-active classical and an online data-driven adaptive control technique are then employed to examine the efficacy of the rocking isolation system. Parameters of the data-driven controller are estimated online in real-time using the Recursive Least Squares approach, which offers simplicity, robustness against faults, and small memory requirements. Numerical simulations are compared with experimental investigations to validate the accuracy of the developed dynamic equations and the performance of the MR dampers and control techniques in mitigating the seismic effects on the examined fluid tank. The MR dampers and semi-active control strategies proved substantial reductions in the uplift displacement of the tank as one of the main causes of damage to these structures under earthquakes.

1. Introduction

Vibrations of fluid and liquid sloshing in partially filled liquid storage tanks either due to the movement of the tank or external excitations are the focus of different research communities. These structures have found crucial applications in a variety of industries including civil structures/infrastructures, nuclear, aerospace, dairy products, water storage, naval, mechanical, transportation, and wine industries [1,2]. When above-ground upright fluid tanks are excited at their base, mainly due to seismic excitations, depending on the material type, flexibility of the tank wall, closure type, and fixity conditions of the tank base, different types of damage could occur to these structures as discussed in [3–7].

Various techniques and devices have been investigated in the literature to reduce the adverse effects of fluid vibrations and sloshing in fluid tanks. A variety of passive, a series of active, and very few cases of semi-active control mechanisms have been proposed in the literature and, in very few cases, tested experimentally for seismic vibration control of fluid tanks. Base isolators in various forms [8] including friction pendulum system (FPS) [9], variable curvature friction pendulum system (VCFPS) [10], multi-phase friction bearing [11], quintuple friction pendulum bearing (QFPB) [12] have been studied. Other passive systems including tuned flexible absorbers [13], U-shaped steel strip dampers [14–16], slip friction connectors [17], resilient slip friction dampers (RSFDs) [18,19], floating roofs [20], and floating roofs equipped with viscous dampers [21] have been proposed. In the category of active and semi-active systems, flexible active floating panels [22,23], active baffle plates and piezoelectric patches [24,25], and magnetorheological (MR) dampers [26] can be mentioned, among others. A comprehensive review of such devices and systems can be found in [27]. The application of MR dampers, as one of the most famous devices in the category of semi-active control mechanisms, for vibration control of legged flexible fluid tanks with fixed base conditions in a horizontal mode was numerically investigated by authors in [28]. Fixity conditions of the tank base to the ground can be regarded as a spectrum having two extreme ends. At one end of the spectrum, the tank is fully fixed to the base while at the other extreme condition, it is unanchored to freely uplift. A series of seismic protection devices proposed for upright fluid tanks offer a kind of vertical flexibility, in some cases referred to as vertical rocking isolation (VRI) [29–31].

When tanks under the base excitations experience uplift, the equations of motion for the dynamic behaviour of the tank become even

* Corresponding author.
E-mail addresses: ehsan.hosseini@autuni.ac.nz (S.E.A. Hosseini), sherif.beskhyroun@aut.ac.nz (S. Beskhyroun).

https://doi.org/10.1016/j.ijepes.2025.111113
Received 25 June 2025; Received in revised form 29 August 2025; Accepted 6 September 2025
Available online 22 September 2025

more complicated than the case that it experiences only lateral vibrations. These equations will be highly dependent on the flexibility of the tank, whether it is legged or flat-based, and the tank's base plate uplift behaviour in the case of flat-based tanks. Pioneering investigations on the uplift behaviour of fluid tanks include the works conducted by Veletsos [32], Veletsos and Tang [33], Haroun and Ellaithy [34], Ishida and Kobayashi [35], and Malhotra and Veletsos [36–38]. Improvements and modifications in the dynamic modelling of uplift for fluid tanks were presented by other researchers [39–42]. In these studies, the main focus is on the modelling of the flexural behaviour of the base plate, inclusion of the added terms to the fundamental dynamics of the system based on the lumped parameter model [43–45], and the added stress levels on the shell [46–49]. In the case of rigid tanks, when the tank experiences uplift under the base excitations, it will in fact be subject to rocking motions as a rigid body. The set of equations developed for such tanks in this section has been inspired by the seminal works of pioneers and researchers who studied the rocking motion of rigid blocks [50–57]. Hence, the idea of rocking rigid structures has been extended to the application of rigid tanks to develop the required equations and then use them for the purpose of vibration control of the coupled system. Due to the rigidity of the tank, the whole fluid-tank system can be modelled as a single lumped mass under a rocking motion. Thus, using the equations presented for rigid tanks [58], the equivalent mass, mass moment of inertia, and height of the lumped mass to the base are calculated. Then, based on the idea of the rocking motion of rigid bodies, the equation of motion for the rigid legged tank is developed. To the best knowledge of the author, this set of equations to represent the dynamic behaviour of such tanks has not been explored in the literature before.

In practice, many systems in the real world have much more complicated dynamics and behaviour that cannot be modelled using closed-form representations. Even if the system's dynamic behaviour can be modelled there would be other challenges such as a high computational burden of a substantially complex formula for multi-physics problems such as fluid tanks for a feasible control application. Additionally, issues including nonlinearities in the system's behaviour, degradation of the system's properties over time, the system's time-varying properties under the applied excitations, and input and output signals' physical constraints, among others, render the application of first-principles-based classical control design impractical and inefficient [59–61]. To overcome these difficulties and enhance the performance of the control system, especially in the long run, a new class of control designs termed Data-Driven Control (DDC) systems come into play. These techniques are divided into two main categories of indirect or model-based DDC and direct or model-free methods [62]. In indirect methods, first based on the observed data a model using system identification techniques is identified for the system under control. Then, based on the identified model, the controller is designed. However, in the direct methods, the system identification step is skipped and the observed data are directly mapped to the desired control action for the system.

A variety of different direct and indirect DDC methods have been studied in the literature [63–65]. Model-free Adaptive Control (MFAC), Iterative Feedback Tuning (IFT), Virtual Reference Tuning (VRF), Iterative Learning Control (ILC), DDC methods based on Behavioral Systems Theory, can be named among others [62,63]. The PID control technique is a widely used strategy in most control applications in industry. This control method may have been the first technique applied in the world of DDC [63,66]. Here, a data-driven adaptive technique based on the PID control strategy is used to control the rigid cylindrical legged tank. Experimental tests over this tank have been conducted in the Structural Engineering Laboratory of Auckland University of Technology. The results of these tests will be described in detail in the next chapter and this subsection is dedicated to the theoretical description of the applied technique.

Considering the literature reviewed above, application of a smart flexible adaptive vertical isolation system for rocking motion of fluid tanks under base excitations such as earthquakes has not been investigated comprehensively, neither numerically nor experimentally. Therefore, a research gap is observed in this field. In this research, a Smart Vertical Isolation System (SVIS) based on the application of MR dampers as smart semi-active systems [67–69] for rocking isolation of the considered rigid legged cylindrical fluid tank under base excitations has been considered. MR damper forces are then incorporated in the developed equations of motion for the system and finally, a set of transfer functions are obtained for vibration control of the system. Using the obtained transfer functions, different control techniques are then developed to examine the performance of the added dampers to the fluid tank to develop a smart vertical rocking isolation system for vibration mitigation of fluid storage tanks. A semi-active online direct DDC method based on an adaptive PID control scheme, herein termed as (ODDAPIDC), is developed to control the rigid cylindrical legged tank. In this scheme, the online data from sensors are received at each time step. Then, based on a set point as the reference and a transfer function of the plant as the model reference, two error values are calculated at each time step. As discussed earlier, in direct DDC methods instead of identifying the plant, the observed data are directly used to design the controller. Therefore, in the adopted control scheme here, the parameters of the PID controller are identified at each time step based on the observed data to satisfy the control objective. Different identification methods have been introduced in the literature to adaptively estimate the controller parameters, including fuzzy logic [70], Predictive Neural Network [71], Chebyshev Neural Network [72], and Monte Carlo based techniques [73,74], among others. Here, an adaptation mechanism using the Recursive Least Squares (RLS) is employed to minimise a cost function based on the estimation error [75–77]. This technique offers promising features including robustness against faults when the system undergoes substantial changes, simplicity of the algorithm for application and modifications for different systems, and small memory requirements [78].

A vertical mode for the implementation of the MR dampers for equipping a legged rigid circular cylindrical fluid tank is considered. This tank was considered in an unanchored condition rocking freely as a rigid body under the base excitations. A set of equations was developed to represent the dynamic behaviour of such a coupled MR-fluid-tank system. A set of numerical examinations was conducted to study the efficacy of MR dampers in mitigating the seismic responses of such a tank. Experimental results of shake table tests conducted over a rigid legged cylindrical fluid tank equipped with MR dampers connected between the legs and the ground vertically to develop a rocking isolation system for fluid tanks based on smart dampers are presented.

2. Dynamic modelling of the coupled system

In this section, the equation of motion for a rigid legged circular cylindrical tank under the base seismic excitations is developed. To the aim of developing the equation of motion for the considered rigid legged tank, the 3-D schematic of the system equipped with MR dampers and the equivalent mechanical representation of the rigid body rocking motion of the coupled system have been illustrated in Figs. 1–2. The cross-sections of the tank cylinder and the legs are shown in Fig. 3.

The non-smooth equation of motion of the system without MR dampers, considering the moment equilibrium around pivot point O, is written as follows,

$$\left.\begin{array}{ll} I'\ddot{\theta} + m'gR'sin(\alpha-\theta) = -m'R'\ddot{U}_g(t)cos(\alpha-\theta), & \theta > 0 \\ I'\ddot{\theta} + m'gR'sin(-\alpha-\theta) = -m'R'\ddot{U}_g(t)cos(-\alpha-\theta), & \theta < 0 \end{array}\right\} \quad (1)$$

$$I' = I_{tot} + m'h'R'cos(\alpha-\theta) \quad (2)$$

$$R' = \sqrt{R_{cy}^2 + h_1^2} \quad (3)$$

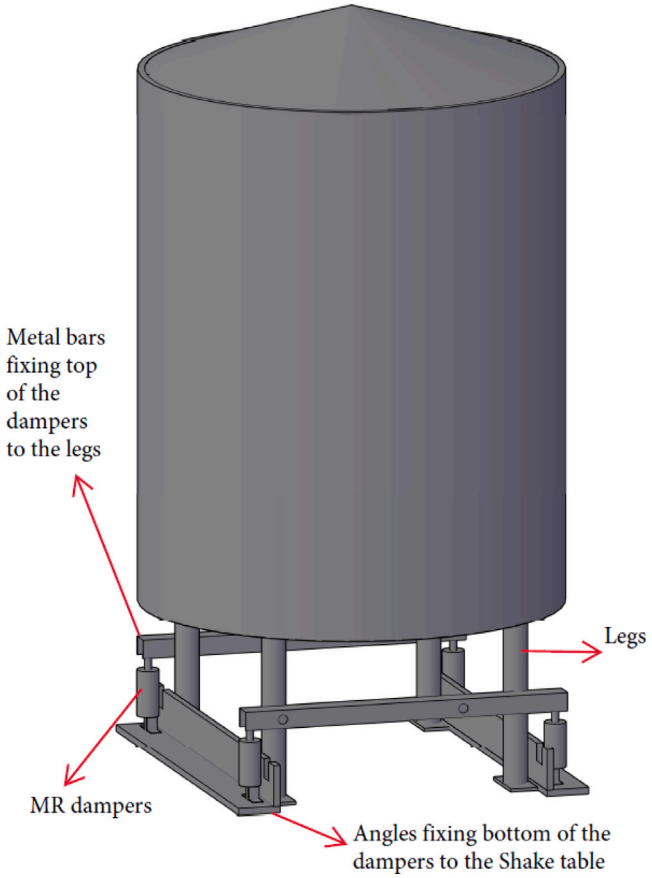

Fig. 1. 3-D Schematic of the rigid legged circular cylindrical tank equipped with MR dampers under uni-directional base excitaions.

$$m' = m_{eff-liq} + m_{tank} \tag{4}$$

$$h' = \frac{m_{eff-liq} h_{eff-liq} + m_{tank}\left[\frac{h_{cy}}{2} + h_{leg}\right]}{m_{eff-liq} + m_{tank}} \tag{5}$$

$$I_{tot} = I_F + I_{cy} \tag{6}$$

$$I_{cy} = m_{tank}\left[\frac{h_{cy}^2}{12} + \frac{R_{cy}^2}{4}\right] \tag{7}$$

$$I_F = A_s I_s \tag{8}$$

$$I_s = m_F\left[\frac{h_l^2}{12} + \frac{R_{cy}^2}{4}\right] \tag{9}$$

In the above equations, θ is the angle of the rigid body rotation, I' the mass moment of inertia of the system, g is the gravitational acceleration, $\ddot{U}_g(t)$ is the ground motion acceleration in g, I_F the mass moment of inertia of the fluid inside the tank, I_s the mass moment of inertia of a solidified liquid inside a cylindrical container, I_{cy} the mass moment of inertia of the tank cylinder, R_{cy} the radius of the cylinder, h_{cy} the height of the tank cylinder, h_l the height of the liquid in the tank, h_{leg} the height of the legs, m_{tank} the mass of the tank without the contained fluid, m_F the mass of the fluid inside the tank, and A_s is a factor that can be conveniently obtained from charts presented in the literature for calculating the equivalent mass moment of inertia of fluid inside rigid cylindrical containers [79]. $m_{eff-liq}$ is the effective equivalent lumped mass of the coupled liquid-tank system while $h_{eff-liq}$ is the height of this mass from the base of the tank. Values of these two parameters can be obtained as below,

$$m_{eff-liq} = M_l \sum_{n=1}^{\infty} A_n \tag{10}$$

$$h_{eff-liq} = \left(\frac{M_l}{m_{eff-liq}}\right) H_l \sum_{n=1}^{\infty} C_n \tag{11}$$

which M_l is the total mass of the fluid in the tank, and A_n represents the below equation,

$$A_n = S\left[\frac{16}{\pi^3(2n-1)^3}\right]\frac{I_1\left[\frac{(2n-1)\pi}{2S}\right]}{\dot{I}_1\left[\frac{(2n-1)\pi}{2S}\right]} \tag{12}$$

$$C_n = \left[1 - \frac{2\times(-1)^{n+1}}{(2n-1)\pi}\right] A_n \tag{13}$$

where S is the tank's aspect ratio (h_l/R_{cy}), $I_1[.]$ is the modified Bessel function of the first kind of order one, and $\dot{I}_1[.]$ is its first derivative. A rotational damping term is defined as below [57],

$$C_\theta = \zeta_\theta m' R'^2 \sqrt{\frac{g}{R'}} \tag{14}$$

where ζ_θ is the rotational damping ratio. Adding the rotational damping term to Eq. (1) and then dividing by the term R' will result,

$$\left.\begin{aligned} \frac{I'}{R'^2}\ddot{\theta} + \zeta_\theta m' \sqrt{\frac{g}{R'}}\dot{\theta} + m'\frac{g}{R'} sin(\alpha-\theta) &= -\frac{m'}{R'}\ddot{U}_g(t)cos(\alpha-\theta), \quad \theta > 0 \\ \frac{I'}{R'^2}\ddot{\theta} + \zeta_\theta m' \sqrt{\frac{g}{R'}}\dot{\theta} + m'\frac{g}{R'} sin(-\alpha-\theta) &= -\frac{m'}{R'}\ddot{U}_g(t)cos(-\alpha-\theta), \quad \theta < 0 \end{aligned}\right\} \tag{15}$$

By defining the "Rocking Frequency Parameter" of the rigid tank as,

$$P' = \sqrt{\frac{g}{R'}} \tag{16}$$

Eq. (15) can be rewritten in a closed form representation as below,

$$\frac{I'}{R'^2}\ddot{\theta} + \zeta_\theta m' P' \dot{\theta} + m' P'^2 sin(\alpha sgn(\theta) - \theta) = -\frac{m' P'^2}{g}\ddot{U}_g(t)cos(\alpha sgn(\theta) - \theta) \tag{17}$$

The non-smooth Equation (17) can be used to determine the time history responses of the system in the uncontrolled case under ground accelerations. Considering a legged tank-fluid system in a practical three-dimensional application, including the applied control mechanism beside each leg of the tank, and incorporating the corresponding control force in the equation of motion,

$$\begin{aligned} &\frac{I'}{R'^2}\ddot{\theta} + \zeta_\theta m' P' \dot{\theta} + m' P'^2 sin(\alpha sgn(\theta) - \theta) \\ &= -\frac{m' P'^2}{g}\ddot{U}_g(t)cos(\alpha sgn(\theta) - \theta) - \frac{4R_{cy}}{R'^2}U_{cont}(t) \end{aligned} \tag{18}$$

To facilitate a control system design for the coupled fluid-tank-MR damper system using the model reference transfer function technique and considering the below approximations for slender tanks under small amounts of rotations,

$$\left.\begin{aligned} &sin(\alpha-\theta) \approx (\alpha-\theta) \\ &cos(\alpha-\theta) \approx 1 \\ &\alpha \approx 2\theta \end{aligned}\right\} \tag{19}$$

Eq. (18) can be linearised to the following equation for $\theta > 0$,

$$\frac{I'}{R'^2}\ddot{\theta} + \zeta_\theta m' P' \dot{\theta} + m' P'^2 \theta = -\frac{m' P'^2}{g}\ddot{U}_g(t) - \frac{4R_{cy}}{R'^2}U_{cont}(t) \tag{20}$$

where $U_{cont}(t)$ is the control force applied to the system. The above system can be regarded as a multi-input single-output (MISO) system with ground motion as the disturbance to the system, while the objective of

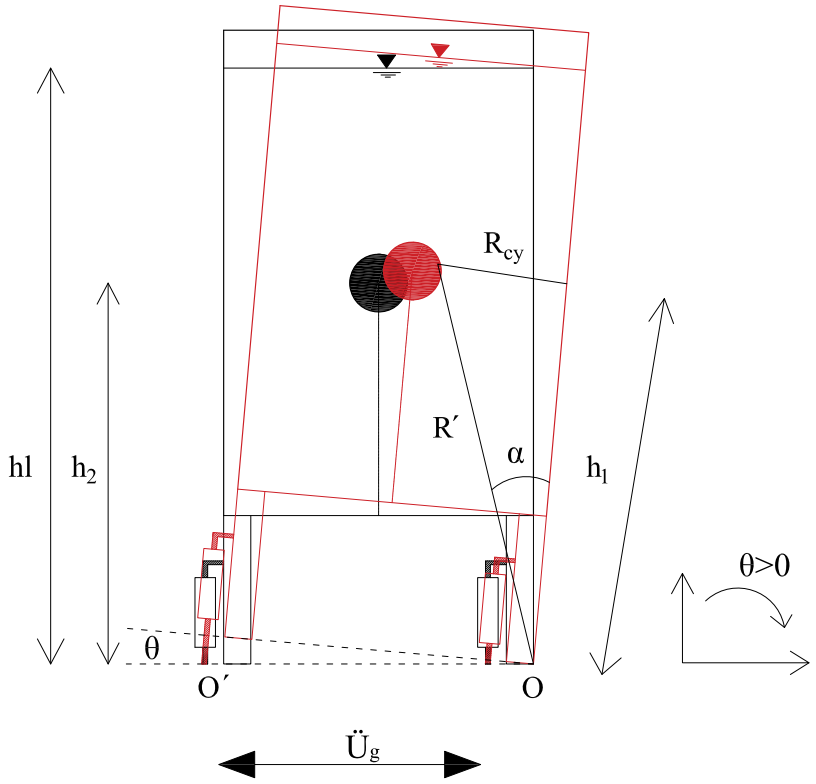

Fig. 2. Rigid body rocking motion of a rigid legged circular cylindrical tank under uni-directional base excitations.

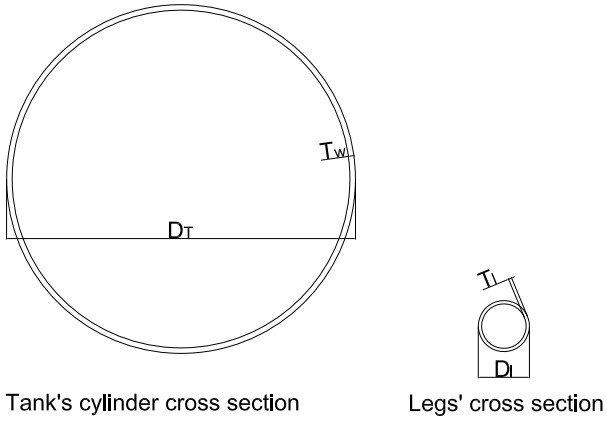

Fig. 3. Cross section of the tank's cylinder and legs.

the control force is to minimise the effects of the input disturbances and maintain the stability of the system. Taking the Laplace transform from both sides of Eq. (20), considering zero initial conditions, gives,

$$\theta(s)\left[\frac{I'}{R'^2}s^2+\zeta_\theta m'P's+m'P'^2\right]=-\frac{m'P'^2}{g}U_g(s)-\frac{4R_{cy}}{R'^2}U_{cont}(s) \tag{21}$$

Thus, the transfer function from input $\ddot{U}_g(t)$ and $U_{cont}(t)$ to the output $\theta(t)$, respectively, would be,

$$H_1(s)=\frac{\theta(s)}{-U_g(s)}=\frac{\frac{m'P'^2}{g}}{\left[\frac{I'}{R'^2}s^2+\zeta_\theta m'P's+m'P'^2\right]} \tag{22}$$

$$H_2(s)=\frac{\theta(s)}{-U_{cont}(s)}=\frac{\frac{4R_{cy}}{R'^2}}{\left[\frac{I'}{R'^2}s^2+\zeta_\theta m'P's+m'P'^2\right]} \tag{23}$$

Using the transfer functions above, a control strategy can be employed to design the control force and satisfy the control objectives. To fulfil the control objectives and minimise the effects of the input disturbance (ground motion) on the considered rigid legged cylindrical tank, two control strategies have been applied. A description of the employed control strategies will be discussed in the next section.

The dynamic behaviour modelling of the MR damper is considered based on the modified Bouc–Wen hysteresis representation. Based on this dynamic modelling, the force produced by the damper is formulated using Eqs. (24)–(29) [80–83],

$$f_{MR}=\alpha z+c_0(\dot{x}_M-\dot{y})+k_0(x_M-y)+k_1(x_M-x_0) \tag{24}$$

$$\dot{z}=-\gamma|\dot{x}_M-\dot{y}|z|z|^{(n-1)}-\beta(\dot{x}_M-\dot{y})|z|^n+A(\dot{x}_M-\dot{y}) \tag{25}$$

$$\dot{y}=\frac{1}{c_0+c_1}\left[\alpha z+c_0\dot{x}_M+k_0(x_M-y)\right] \tag{26}$$

$$\alpha(\tau)=\alpha_a+\alpha_b\tau \tag{27}$$

$$c_1(\tau)=c_{1a}+c_{1b}\tau \tag{28}$$

$$c_0(\tau)=c_{0a}+c_{0b}\tau \tag{29}$$

where α_a, α_b, c_{1a}, c_{1b}, c_{0a}, c_{0b}, μ, k_0, k_1, A, β, γ, x_0, and n are the 14 parameters associated with the modified Bouc–Wen model, and x_M and $\dot{x}_M$ are the displacement and velocity of the MR damper. τ is a first-order filter with a transfer function in the s-domain expressed in Eq. (30) that is applied over the decided voltage v to the damper,

$$\tau(s)=\frac{\mu}{s+\mu} \tag{30}$$

This filter in the z-domain has been presented in Appendix.

3. Vibration control scheme

3.1. Classical PID

The PID control strategy is one of the widely applied control techniques for various applications. This control strategy has proved to be simple, robust, effective, and applicable to a broad class of industrial systems [84,85]. This technique has been used for control design of industrial processes [86], robotic manipulators [87,88], biomedical applications [89,90], electric drives and power applications [91], and mechanical and civil engineering structures [92,93], to name but a few.

The PID control force in the parallel form is written as below,

$$U_{PID}(t) = K_P\left[e(t) + \frac{1}{T_i}\int_0^t e(t)\,dt + T_d\frac{de(t)}{dt}\right] \tag{31}$$

where $e(t)$ is the error function defined as the difference between the output and the reference. The Laplace transform of the above equation would be as follows,

$$U_{PID}(s) = U_P(s) + U_I(s) + U_D(s) \tag{32}$$

and the controller gain would be,

$$K_{PID}(s) = K_P + \frac{K_P}{T_i}(\frac{1}{s}) + K_P T_d s \tag{33}$$

Considering the below relations,

$$K_I = \frac{K_P}{T_i}, K_D = K_P T_d \tag{34}$$

Eqs. (32) and (33) can be rewritten as Eqs. (35) and (36), respectively,

$$U_{PID}(t) = K_P e(t) + K_I\int_0^t e(t)\,dt + K_D\frac{de(t)}{dt} \tag{35}$$

$$K_{PID}(s) = K_P + K_I(\frac{1}{s}) + K_D s \tag{36}$$

where K_P, K_I, K_D, T_i, T_d, and $e(t)$ are the proportional gain, integral gain, derivative gain, integral time constant, derivative time constant, and the error between the reference and the output, respectively. Since the process usually contains noise, a low-pass filtered derivative instead of the pure derivative is applied. In this case, the control force in Eq. (32) would be reformulated as follows,

$$U_{PID}(s) = U_P(s) + U_I(s) + U_{D-LPF}(s) \tag{37}$$

where the filtered derivative term would be in the below form,

$$U_{D-LPF} = K_D\left[\frac{s}{T_f s + 1}\right] \tag{38}$$

where T_f is the filter time constant.

3.2. Energy dissipation

This control strategy is in fact a variation of the decentralised bang–bang control technique [93–95]. In this technique, only the measurements of the damper's force and velocity are required. This strategy benefits from a very simple formula and ensures the command voltage is at its maximum value when the dampers' force is dissipating energy and is at its minimum when the force is not dissipating. The Lyapunov function representing the total energy of the structure is written as below,

$$Y = \frac{1}{2}X_{str}^T K_{str} X + \frac{1}{2}X_{str}^T M_{str}\dot{X}_{str} \tag{39}$$

where X_{str}, $\dot{X}_{str}$, M_{str}, and K_{str}, are the displacement and velocity vector, mass, and stiffness of the structural system. Having the MR damper connected between the ground and the system, to maximise the rate of change of the energy dissipation, the below control law is applied which directly affects the energy of the system,

$$v_{MR}^{Eng} = V_{max,MR}H\{(-\dot{X}_{MR}^T)f_{MR}\} \tag{40}$$

where $\dot{X}_{MR}^T$ is the transpose of the relative velocity of the MR damper. The advantage of this technique in the current application is when the damper is connected between the ground the tank's base or legs only the absolute velocity of the damper is needed. This measurement can be obtained through applying a proper transfer function to the measurements of the accelerometers' data.

3.3. Online data-driven adaptive PID

In the applied data-driven control technique, an adaptation mechanism estimates the parameters of the PID controller online for the next step of the control action. Finally, the calculated control force is sent to the clipping algorithm to decide the input voltage to the MR damper. The schematic of the control design block diagram is shown in Fig. 4.

In Fig. 4, Plant is the sysme to be controlled in this study, i.e. the fluid tank, adaptation mechanism to update the parameters of the adaptive PID (APID) controller online using the observed data from sensors is the RLS identification process, Reference Model is the transfer function of the system, i.e. $H_1(s)$ or $H_2(s)$ which work as the reference model for the DDC control system here, e_{rl} and e_{st} are the real error between received data from the sensors and the estimated error between the observed data and estimated response of the system, respectively, U_{cont} is the online DDC-APID control, r is the reference, Y_{mrd} and Y_{est} are the measured and the desired estimated responses of the plant, respectively, X_{MR} and $\dot{X}_{MR}$ are the displacement and velocity of the MR damper, θ_p is the vector of identified parameters of the PID controller from the adaptation mechanism, LPF is a Low Pass Filter over these parameters, and F_{MR} and V_{MR} are the MR damper calculated force and the decided voltage to the damper based on the Clipping algorithm for the next time step in the online control process of teh system. Therefore, the author terms this control methodology as an Online Data-Driven Adaptive PID-Clipping control (ODDAPIDC) methodology developed for semi-active control of rigid legged cylindrical fluid storage tanks equipped with MR dampers in this study.

3.4. Recursive least squares adaptive PID control technique

In this technique, a tracking error is defined as the difference between the real output of the plant (measured by the sensory system) and the desired estimated output from the model reference. The RLS strategy tries to converge this error to zero asymptotically. Here this tracking error is written as below,

$$\zeta_{RLS}(t) = Y_{mrd}(t) - Y_{est}(t) \rightarrow 0 \tag{41}$$

$$Y_{mrd}(t) = r(t) - e_{rl}(t) \tag{42}$$

$$Y_{est}(t) = H_M(s)r(t) \tag{43}$$

Therefore, to satisfy Eq. (41),

$$H_M(s)r(t) = r(t) - e_{rl}(t) \tag{44}$$

where $H_M(s)$ is the transfer function of the model reference. Considering a PID control gain with a filtered derivative action that counteracts the undesirable noise amplification as follows,

$$C_{PID}(s) = K_P(s) + K_I(s)\frac{1}{s} + K_D\frac{s}{T_f(s)+1} \tag{45}$$

it is obtained,

$$U_{cont}(s) = C_{PID}(s)e_{rl}(s) \tag{46}$$

which in discrete time and the z-domain would be,

$$U_{cont}(z) = C_{PID}(z)e_{rl} \tag{47}$$

Writing Eq. (44) and multiplying both sides of it by the controller gain $C_{PID}(z)$ yields,

$$C_{PID}(z)H_M(z)r = C_{PID}(z)(r - e_{rl}) \tag{48}$$

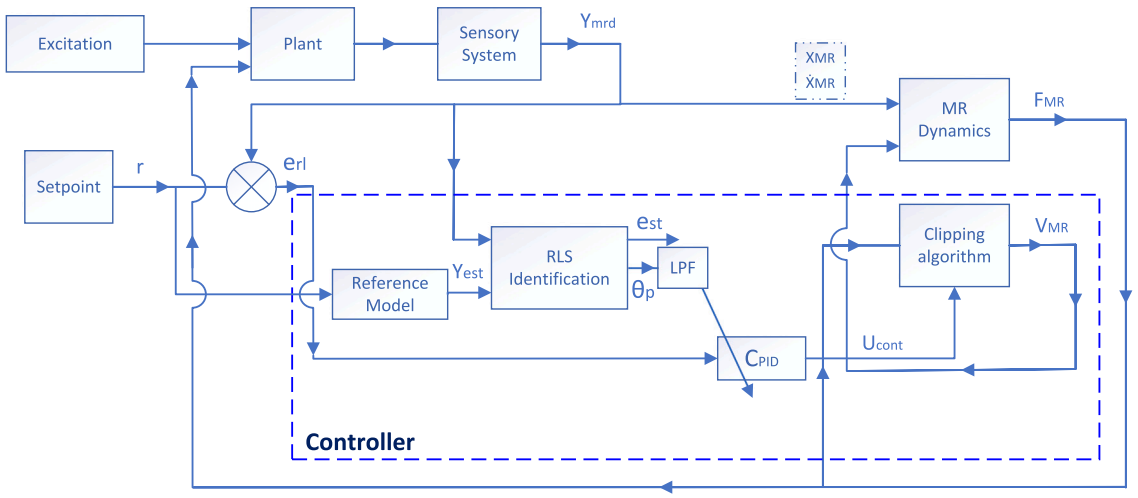

Fig. 4. Schematic of the control design block diagram for semi-active control of the rigid legged cylindrical fluid tank.

Using Eq. (48) and some mathematical manipulations, the tracking error of the RLS technique for the current approach can be written as below,

$$\zeta_{RLS} = U_{cont} - C_{PID}(z)(1 - H_M(z))r \tag{49}$$

Having the tracking error, the cost function of RLS is regarded as follows to satisfy the convergence of the plant output to the desired one,

$$J_{RLS}(k) = \frac{1}{N}\sum_{i=0}^{N-1} \zeta_{RLS}^T(k-i)\zeta_{RLS}(k-i) \tag{50}$$

The controller gain $C_{PID}(z)$ is rewritten as below,

$$C_{PID}(z) = \Theta_{PID}^T \Phi_{PID}(z) \tag{51}$$

where Θ_{PID}^T are the controller parameters to be identified at each time step using the RLS technique,

$$\Theta_{PID}^T = \begin{bmatrix} K_P & K_I & K_D \end{bmatrix} \in \mathbb{R} \tag{52}$$

and $\Phi_{PID}(z)$ using the backward Euler method can be formulated as [96–98],

$$\Phi_{PID}(z) = \begin{bmatrix} 1 & \frac{\tau_s z}{z-1} & \frac{z-1}{(T_f+\tau_s)z - T_f} \end{bmatrix}^T \tag{53}$$

where τ_s and T_f are the sampling time and filtered-derivative time constant, respectively. Substituting Eq. (51) into Eq. (49) and defining,

$$\Phi_{PID,rf} = \Phi_{PID}(z)(1 - H_M(z))r \tag{54}$$

the equation of the tracking error in a step-wise manner can be written as,

$$\zeta_{RLS}(k) = U_{cont}(k) - \Theta_{PID}^T(k-1)\Phi_{PID,rf}(k) \tag{55}$$

Finally, the estimated parameters of the controller using the RLS technique, i.e. the $\Theta_{PID}(k)$, are passed through a Low Pass Filter (LPF) to account for rapid changes in the plant's characteristics [76]. The transfer function of this filter in the z-domain is written as follows,

$$H_{LPF}(z) = \frac{\beta_f}{z + \beta_f - 1}, \qquad 0 \le \beta_f \le 1 \tag{56}$$

It is important to mention that incorporating Eq. (55) in the cost function of the RLS algorithm will result in the process of estimation and updating the controller's parameters online in an adaptive manner at each time step by the Θ_{PID} factor, depending on the previous one. To ensure the stability of the control technique, asymptotic convergence of the tracking error to zero, and avoiding the disturbing effects of the parametric variations in both the identification process and the system itself, the RLS algorithm using the forgetting factor strategy is applied [76,78]. Using this approach,

$$\Theta_{PID}^T(k) = \Theta_{PID}^T(k-1) + K_{RLS}(k)\left[U_{cont}(k) - \Theta_{PID}^T(k-1)\Phi_{PID,rf}(k)\right] \tag{57}$$

K_{RLS} is the adaptation gain vector of the RLS technique that is formulated according to the below equation,

$$K_{RLS}(k) = \frac{\Phi_{PID,rf}^T(k)P_{RLS}(k-1)}{\Lambda_{RLS} + \Phi_{PID,rf}^T P_{RLS}(k-1)\Phi_{PID,rf}}, \quad 0 < \Lambda_{RLS} < 1 \tag{58}$$

In the above equation, P_{RLS} is the covariance matrix and Λ_{RLS} is the forgetting factor. The covariance matrix is written as follows,

$$P_{RLS}(k) = P_{RLS}(k-1) - K_{RLS}(k)P_{RLS}(k-1)\Phi_{PID,rf} \tag{59}$$

Using the developed formulations, techniques, and approaches, numerical simulations, and experimental results are presented in the next sections to examine the efficiency of the MR damper on the dynamic behaviour of the legged fluid tank under the base excitations.

3.5. Semi-active controller

When employing the classical and data-driven adaptive PID control approaches, the control signal using the secondary controller would be acquired using Eq. (60) [82,99–101],

$$v_{MR} = V_{max,MR} H\{(U_{Cont} - f_{MR})f_{MR}\} \tag{60}$$

where $V_{max,MR}$ is the maximum voltage that can be commanded to the damper which depends on the capacity and specifications of the damper, $H\{.\}$ is the Heaviside function, and U_{Cont} is the desirable control force decided by the selected control laws and strategies. A modified version of the clipping algorithm stated in Eq. (60) selects any values between 0 and $V_{max,MR}$. This technique is written as follows [102–105],

$$v_{MR}^{mod} = V_{d,MR} H\{(U_{Cont} - f_{MR})f_{MR}\} \tag{61}$$

where v_{MR}^{mod} is the voltage decided in the modified technique, and $V_{d,MR}$ is decided based on the inequalities in Eq. (62),

$$V_{d,MR} = \begin{cases} V_{max,MR}, & |U_{Cont}| > f_{max,MR} \\ \frac{V_{max,MR}}{f_{max,MR}}|U_{Cont}|, & |U_{Cont}| \le f_{max,MR} \end{cases} \tag{62}$$

where $f_{max,MR}$ is the maximum capacity of the MR damper.

Fig. 5. Experimental setup of the tank with MR dampers.

Table 1
Geometrical and hydrodynamic characteristics of the rigid legged circular cylindrical fluid tank.

Parameter	Value	Parameter	Value
h_{tot}	1332 (mm)	A_n	0.8015
h_{leg}	400 (mm)	B_n	0.4294
h_{cy}	932 (mm)	C_n	0.3442
M_{tot}	580 (kg)	$h_{eff-liq}$	400 (mm)
D_{leg}	47.95 (mm)	R'	571.7 (mm)
R_{cy}	389.93 (mm)	I_F	9 829 700 (kg mm^2)
S	2.33	I_s	49 148 300 (kg mm^2)

Table 2
Parameters of the Bouc–Wen model of the MR damper.

Parameter	Value	Parameter	Value
α_a	1921.141 (N/m)	k_0	1940.405 (N/m)
α_b	5882.51 (N/V m)	k_1	1.751268 (N/m)
c_{1a}	2089.263 (N s/m)	A	155.32
c_{1b}	14 384.918 (N s/V m)	β	36 332.07 (m^{-2})
c_{0a}	651.4718 (N s/m)	γ	36 332.07 (m^{-2})
c_{0b}	1043.7559 (N s/V m)	x_0	0.00 (m)
μ	60 (s^{-1})	n	2

4. Results and discussion

4.1. System properties

This section presents the experimental results of shaking table tests over a legged rigid stainless steel circular cylindrical liquid tank equipped with four MR dampers under rocking motions. This tank is made of stainless steel and has a very rigid body with a thickness of around 2 cm. Other geometrical specifications of the tank are given in Table 1. Details of these tests and data analysis of the experimental results are described in the below sub-sections. In this table, h_{tot}, M_{tot}, and D_{leg} are the total height and mass of the tank filled with water, and the diameter of the legs, respectively. The rest of the parameters in this table were already discussed in Section 2. Moreover, the rotational damping ratio ζ_θ was considered as 5%.

The considered MR damper in this study has a capacity of around 2.45 kN, and the input voltage to the damper is regarded in the range of 0 to 3 V. The MR damper model regarded in this study is RD-8041-1 (long stroke). The parameters of the modified Bouc–Wen model for the MR damper are considered as presented in Table 2 which have been experimentally obtained and verified in previous investigations [106].

4.2. Experimental setup

A rigid legged stainless steel circular cylindrical liquid tank was set up freely over the shake table in the Structural Engineering Laboratory of the Auckland University of Technology (AUT). This tank was filled with water. The shake table platform is a unidirectional table with dimensions of 4000 mm by 2896 mm and a maximum horizontal stroke of ±200 mm, run by the Shore Western controller. The maximum payload of the table is 1 ton and it is capable of producing accelerations up to 2g. The fluid tank and the MR damper were installed over the shake table in two scenarios. In the first scenario, the tank was installed over the shake table without the MR dampers connected to its legs. This tank was tested for a series of swept-sine as well as the selected ground motions with different Peak Ground Acceleration (PGA) scales. The purpose of the swept-sine tests was to detect the natural frequencies of the legged rigid circular cylindrical stainless steel fluid tank while the aim of testing for ground motions was to compare results with the controlled tank. In the second scenario, the same tank was equipped with four MR dampers, each installed beside one of the legs. Again the tank was tested under the same ground motions. Finally, the results of the vibration responses of the system including the uplift displacements of the tank, uplift relative accelerations of the legs, and the lateral absolute accelerations of the tank body in two cases were compared to examine the efficacy of the dampers in attenuating the seismic responses of the tank under the base excitations. Fig. 5 shows the details of the installation setup for the fluid tank equipped with MR dampers over the shake table to provide rocking isolation. The supporting platform for protecting the tank can also be seen this figure.

4.3. Instrumentation of rigid fluid tank-MR system

The fluid tank was instrumented using different sensors including accelerometers, Linear Variable Differential Transformers (LVDT's), and MR dampers as shown in Fig. 6. To command the calculated voltage at each time step using the control algorithm to the damper

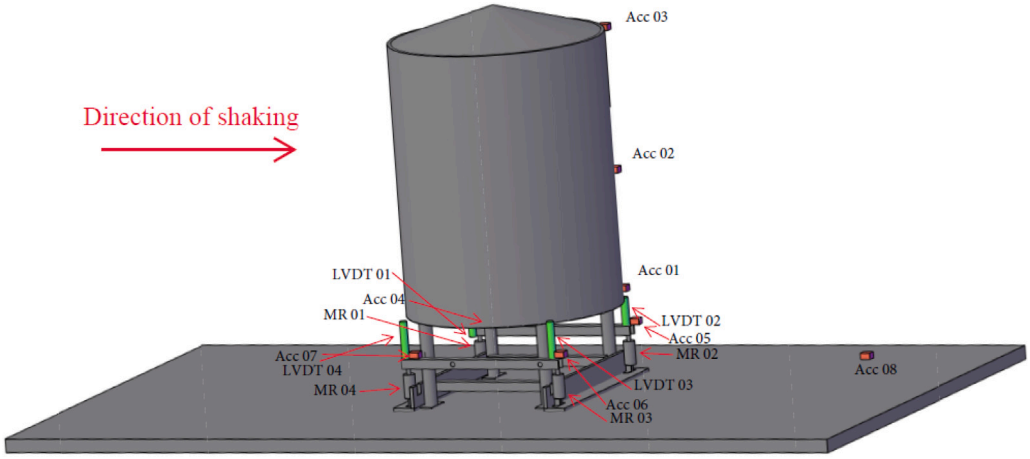

Fig. 6. An iso-geometric view of the instrumentation of the rigid fluid tank-MR damper for data acquisition and control.

a Pulse Width Modulator (PWM) control box was designed by the technicians of the Auckland University of Technology (AUT) as seen in Fig. 7. Moreover, a software platform based on SIMULINK-MATLAB was developed for data acquisition and online control of the system based on the developed control techniques. The block diagram for this software has been illustrated in Fig. 8.

This software has different capabilities, including data acquisition from the sensory system for different types of sensors, online control using different control techniques which can easily be switched, real-time output saving, and data visualisation. Eight accelerometers, Acc 01 to Acc 08 were utilised. Acc 01 to Acc 03 were connected to the bottom, mid-height, and top of the tank, respectively, to measure the lateral accelerations of the fluid tank. Acc 04 to Acc 07 were connected beside each leg very close to the position of each MR damper and LVDT to measure the upward accelerations of the legs. LVDT 01 to LVDT 04 were installed to measure the uplift displacements of the legs and MR 01 to MR 04 were installed beside the legs to control the system. Moreover, four PWM control boxes were applied to transmit the analog output from the DAQ and command the control voltage signal to the MR dampers. The National Instruments Data Acquisition (NI DAQ) hardware was employed for receiving and logging the analog input signals from the sensors and sending the analog output voltage command signal to the dampers. A sampling rate of 50 Hz was used for the process of simultaneous data acquisition and control.

As shown in Fig. 8 real-time data from LVDT's are used for the process of feedback in the control process. Different control methods were employed to examine the performance of the controlled system. Voltages sent to the PWM control boxes from the control design to be transmitted to the MR dampers were bound in the range of 0–3 V.

4.4. Experimental and numerical results

The seismic records of seven past prominent earthquakes including the 1979 El Centro, the 1999 Kocaeli, the 1990 Manjil, the 1995 Kobe, the 1989 Loma Prieta, and the 2011 Christchurch, and the 1978 Tabas were used for experimental examinations. Records of the selected ground motions were obtained from the Pacific Earthquake Engineering Research Center (PEER), Next Generation Attenuation (NGA-West2) database for historical earthquake recrods [107], (https://ngawest2.berkeley.edu/). Each record was scaled using SeismoSignal [108] to specific Peak Ground Acceleration (PGA) values. Displacement time histories in millimetres units were used for each scaled ground motion and were given to the shake table to produce the excitations. A time step of 0.02 s was used to produce time histories using the shake table. Details of each ground motion, including the event name, station, year, fault type, mechanism, magnitude (M_w), and PGA have been

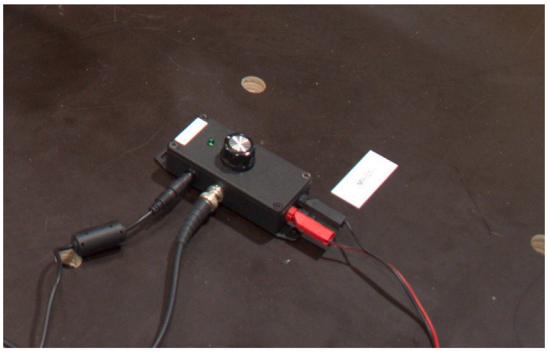

Fig. 7. Pulse Width Modulator (PWM) control box developed for commanding voltage to the MR dampers.

presented in Table 3. The legged rigid fluid tank was controlled under different scales of the selected ground motions and for various control techniques. The applied scaled ground motions include Christchurch 0.438g (≈92% of full-scale), Kobe 0.525g (63% of full-scale), and Loma Prieta 0.512g (3× full-scale). The applied control methods consist of two passive modes including the Passive Off (constant zero voltage to the damper) and Passive On (constant 3 V to the damper), and different semi-active techniques including the energy dissipation method and a series of many other different techniques.

Using the formulae developed in Section 2 for the dynamic behaviour of rocking rigid legged cylindrical tank, and control techniques described in Section 3, numerical simulations for the uncontrolled and controlled system utilising MR dampers were conducted using SIMULINK - MATLAB. Numerical results were polluted with White Gaussian Noise (WGN) with a signal-to-noise ratio (SNR) of 1 dB to simulate the practical applications in the presence of noise. Numerical results were compared to experimental ones to examine the performance of the developed equations and applied control techniques.

A comparison between the experimental and theoretical peak uplift displacements of the tank under the selected earthquakes in the uncontrolled case has been presented in Table 4. In the presented figures and tables for the results, channels $CH10$ and $CH11$ represent the $LVDT02$ and $LVDT03$ sensors, respectively, measuring the uplift displacements of the tank at pivot point O corresponding to rotations of the tank around pivot point $O\prime$ ($\theta < 0$) which were found to be the largest among those of other displacement sensors. After examining the experimental results of some primary tests, ground motions with certain PGA scales were found to create enough uplift displacements in the system for the MR dampers to come into action and start dissipating the external

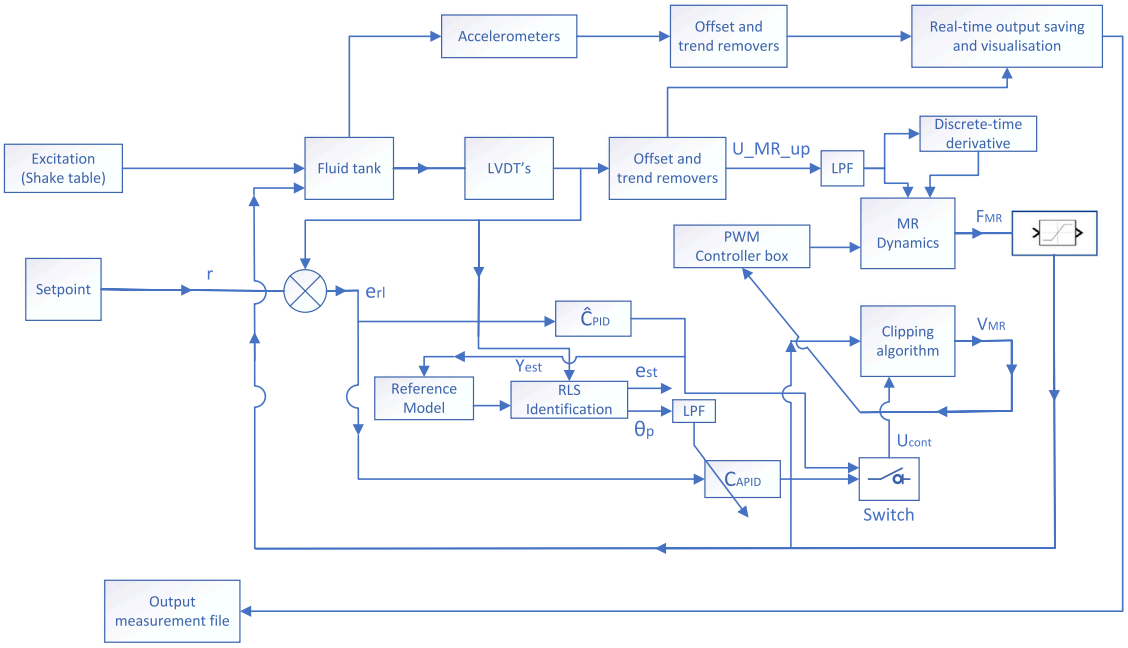

Fig. 8. Data acquisition and online control system block diagram of the developed software platform.

Table 3
Details of the earthquake records used for seismic ground motion tests of the fluid storage tank.

Event	Station	Year	Fault type	Mechanism	M_w	PGA (g)
Loma Prieta	APEEL 2E Hayward Muir Sch	1989	Far-fault	Reverse-oblique	6.93	0.171
Kobe	KJMA	1995	Near-fault, Pulse-like	Strike-slip	6.9	0.834
Christchurch	Cathedral college	2011	Near-fault	Reverse oblique	6.2	0.478

energy. Thus, these ground motions which include Christchurch $0.438g$, Kobe $0.525g$, and Loma Prieta $0.512g$ were set as the focus of controlled system tests. Experimental results of the peak uplift displacements of the uncontrolled and controlled system for a series of selected applied controllers have been listed in Table 5.

Fig. 9 illustrates the comparison between the experimental tests and theoretical simulations for the legged tank in the uncontrolled case under the Christchurch 2011 earthquake. Different controllers were applied to the system, including passive controllers, i.e. the Passive On and Passive Off, and the remaining controllers were the semi-active model-based and online data-driven adaptive controllers. Various model-based and data-driven controllers were applied to the system. A selection of the applied control techniques have been presented in Table 5. Model-based controllers presented in this table include PIDCLIP05, PIDCLIP06, PIDCLIP09, and PIDCLIP10 for the standard PID-clipping technique and PIDMCLIP03 for the PID-modified-clipping approach. For the online data-driven adaptive PID techniques, ODDAPIDC01 and ODDAPIDC06 using the standard clipping and ODDAPIDMC01 and ODDAPIDMC02 for the modified clipping control have been presented. It is noteworthy that the PID control parameters for the model transfer function in the case of model-based techniques and for the model reference transfer function in the case of data-driven approaches were obtained using the PID tuner toolbox of MATLAB R2023b. Since a variety of controllers and transfer functions were examined, only those whose results have been presented in this research have been appeared in the Appendix. The discrete transfer functions $H_1(z)$ and $H_2(z)$ in this Appendix have been obtained by discretisation of Eqs. (22) and (23) considering a time interval of 0.02 s, while $H_4(z)$ has been acquired by discretisation of Eq. (22) considering a time interval of 0.005 s. The applied control methods, controller parameters, and different applied digital filters can be found in Appendix.

Comparisons between the numerical and experimental results for both cases of controlled and uncontrolled systems under the Christchurch $0.438g$ have been illustrated in Figs. 10–11 for the controller PIDCLIP05. Experimental results of the uncontrolled system versus the controlled system, as well as the results of different controllers, under different ground motion tests, have been illustrated in Figs. 12–15. The control system design implementation was achieved using the developed software platform via SIMULINK which receives signals from the National Instruments Data Acquisition (NI-DAQ) system, analyses and processes them using the developed control procedures, and commands them to the PWM boxes.

A comparison between the results of numerical evaluations using the developed equations for modelling the dynamic behaviour of the rocking rigid legged circular cylindrical tank under ground accelerations with that of experimental results has been presented in Table 4. As shown in this table, depending on the applied earthquake, the estimation error varies in the range of 6%–13%. As seen in Figs. 9 and 10, the numerical and experimental peak uplift responses of the system either in the controlled or uncontrolled cases occur at different time instances which is attributed to the realistic laboratory test conditions for start and finish time for each experimental test. Moreover, as demonstrated in these figures, contrary to the experimental results, in the numerical case, there are more fluctuations in the uplift response of the fluid tank from the beginning of the uplift (rotation of the system) until it reaches back to the settling conditions again. The non-smooth equations of motion for the dynamic behaviour of the rigid legged circular cylindrical fluid tank, which experiences rocking motions under base accelerations in this study, were developed by inspiration from pioneering works in this field [50–54,57]. The developed equations in these works, the dissipation of energy due to inelastic impact, and the expected consequent number of impacts of the rigid block on the surface are for the rocking motion of rigid blocks having a completely uniform rectangular geometry that is different from the fluid tank system considered in this research. Considering the fact that similar

Table 4
Experimental and theoretical peak uplift responses of the uncontrolled rigid legged tank-liquid system under different applied ground motion tests.

Uplift	Christchurch 0.438 g	Kobe 0.525 g	Loma Prieta 0.512 g
Theoretical (mm)	14.50	10.50	11.10
Experimental (mm)	15.80	11.13	12.55
Estimation error (%)	8.97	6.00	13.06

Table 5
Experimental peak uplift responses of the rigid legged tank-liquid-MR damper system under the selected ground motions for different control techniques.

Uplift response	Control technique	Christchurch 0.438 g	Kobe 0.525 g	Loma Prieta 0.512 g
Uncontrolled system				
U_{CH10} (mm)	Uncontrolled	15.80	11.13	12.55
Passive control tests				
U_{CH10} (mm)	Passive off	7.51	7.93	6.97
	Passive on	3.83	4.19	2.19
Semi-active energy dissipation clipping controller				
U_{CH10} (mm)	Energy dissipation	5.90	6.18	6.80
Semi-active model-based PID standard-clipping controllers				
U_{CH10} (mm)	PIDCLIP05	6.77	6.49	5.34
	PIDCLIP06	6.53	6.47	6.96
	PIDCLIP09	3.18	4.05	4.58
	PIDCLIP10	2.75	3.84	3.28
Semi-active model-based PID modified-clipping controllers				
U_{CH10} (mm)	PIDMCLIP03	3.71	4.76	3.31
Semi-active online data-driven adaptive PID standard clipping controllers				
U_{CH10} (mm)	ODDAPIDC01	2.36	3.55	3.52
	ODDAPIDC06	4.62	4.15	3.08
Semi-active online data-driven adaptive PID modified-clipping controllers				
U_{CH10} (mm)	ODDAPIDMC01	2.69	3.40	–
	ODDAPIDMC02	2.59	4.42	3.89

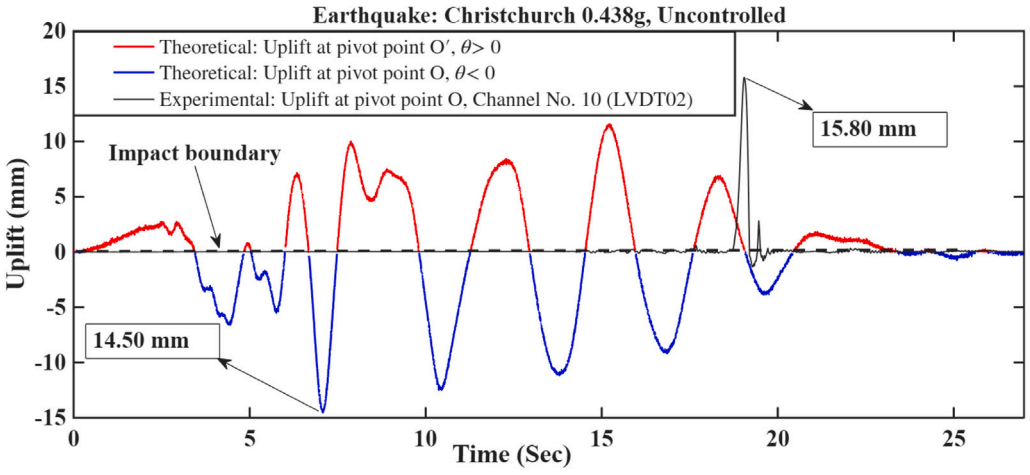

Fig. 9. Experimental and theoretical uplift displacement comparison of the tank without MR dampers (uncontrolled system) under the Christchurch 2011, 0.438 g.

experimental investigations on the rigid legged circular cylindrical fluid tanks are scarce in the literature, the current study shows a verification of the accuracy of the developed equations and sets a foundation for future research in this field.

Examining Table 5 and Figs. 11–15 for the performance of different passive and semiactive model-based and data-driven controllers shows in the case that the dampers are working in a Passive Off mode, they have reduced the uplift displacements of the tank between 29% under the Kobe 0.525g to 52% under the Christchurch 0.438g. In the Passive On mode, uplift responses of the tank have been reduced between 62%–83%. Finally, in the case of applying the selected semi-active controllers, uplift responses of the tank have been attenuated in the range of 44%–85% depending on the type of the controller and the applied ground motion. It is noteworthy that in some of the figures representing the experimental results of tests using different controllers or comparative figures between the uncontrolled system and controlled system using different techniques, there are time differences among different plots. For instance, the peaks of the uplift displacement time history occurred at different time instances under different test runs. These differences are due to the inevitable different start and stop times for running the tests, which resulted in some time differences in the

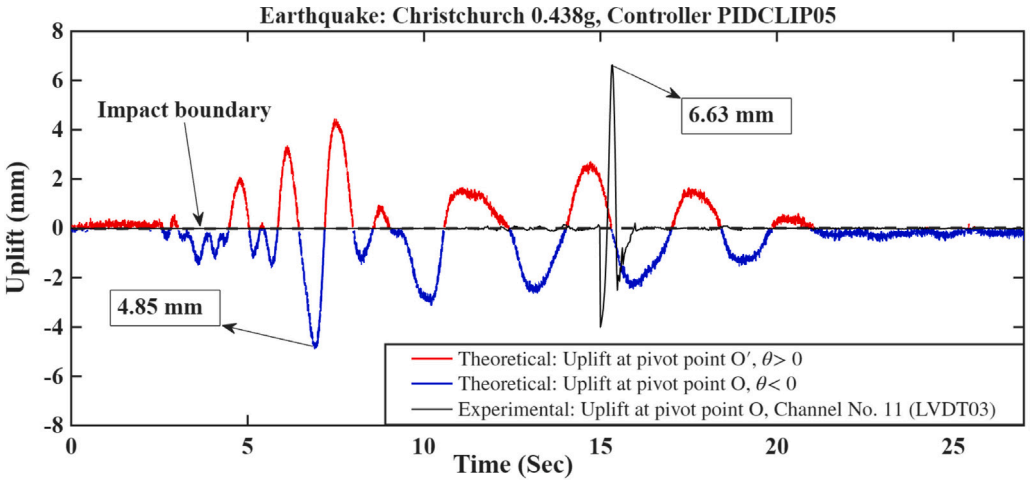

Fig. 10. Experimental and theoretical uplift displacement comparison of the tank with MR dampers under the Christchurch 2011, 0.438 g for controller PIDCLIP05.

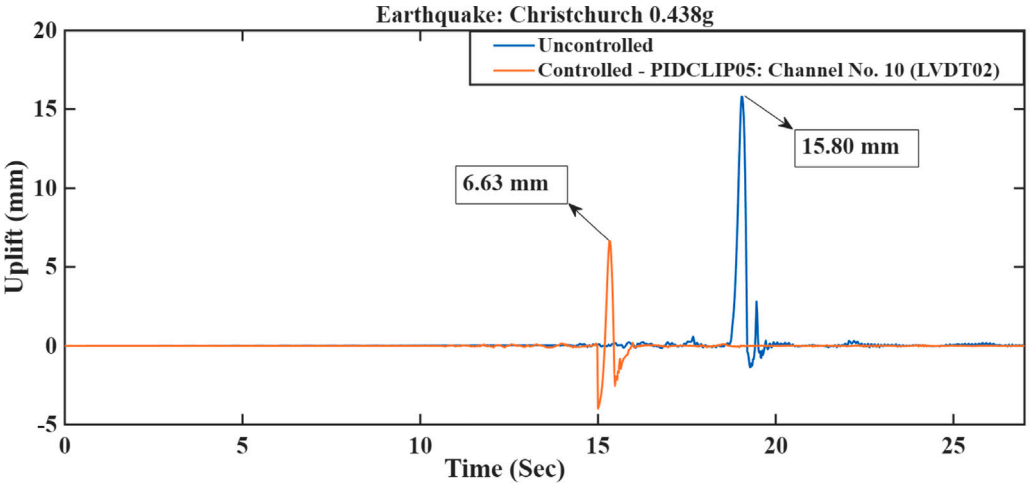

Fig. 11. Uplift displacement comparison between experimental results of the controlled system using PIDCLIP05 controller and the uncontrolled tank under the Christchurch 2011, 0.438 g.

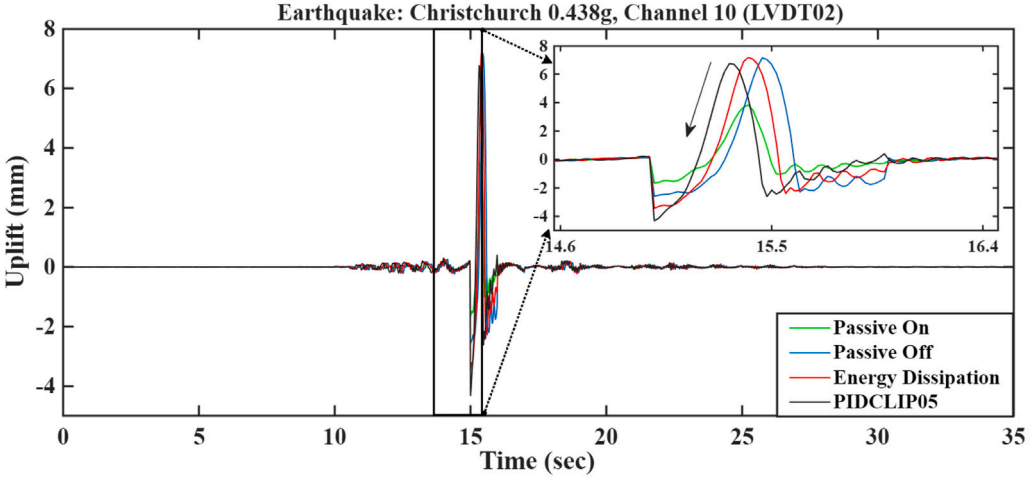

Fig. 12. Uplift displacement comparison between experimental results of two passive and two semi-active controllers under the Christchurch 2011, 0.438 g.

measurements of the sensors at each test during the experiments. Results of Table 5 show that semi-active control strategies using standard and modified Clipping approaches result in almost the same level of performance for the controlled system design. There were found some instances for which the standard Clipping technique resulted in more reductions in the structural responses of the system. The developed online data-driven adaptive controllers were able to follow the same performance indices as that of the model-based controllers and even

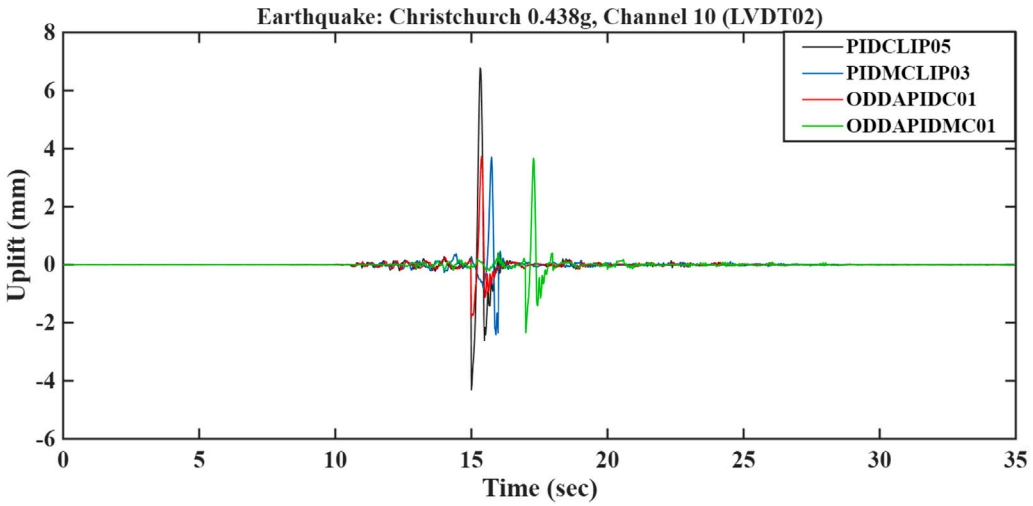

Fig. 13. Uplift displacement comparison between experimental results of several semi-active model-based and online data-driven adaptive controllers using standard and modified Clipping technique under the Christchurch 2011, 0.438 g.

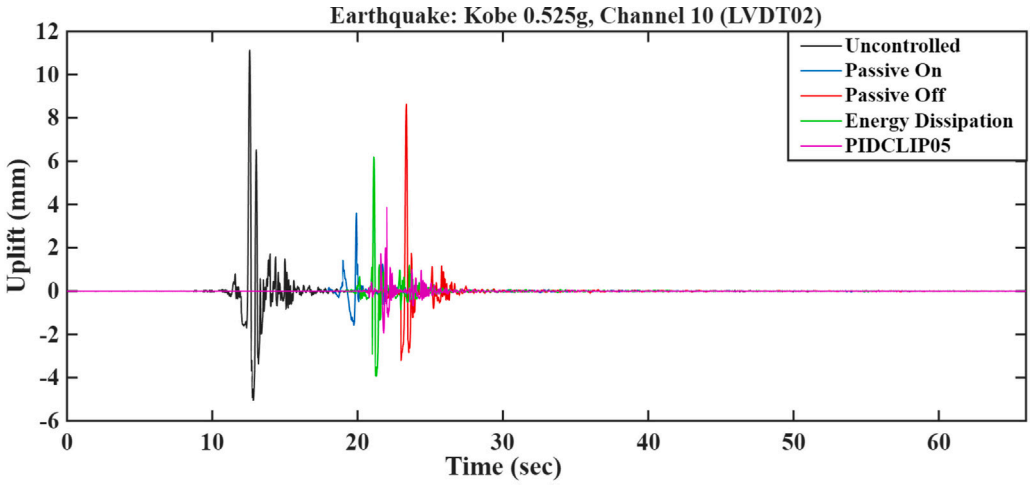

Fig. 14. Uplift displacement comparison between experimental results of uncontrolled and controlled system by passive and semi-active model-based controllers under the Kobe 1995, 0.525 g.

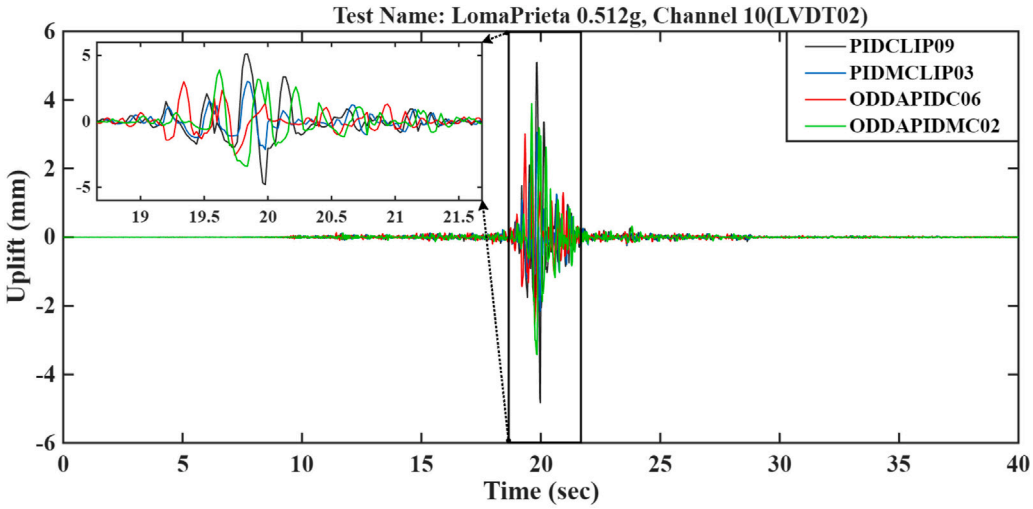

Fig. 15. Uplift displacement comparison between experimental results of the controlled system with several model-based and online data-driven adaptive semi-active controllers using the standard and modified Clipping technique under the Loma Prieta 1989, 0.512 g.

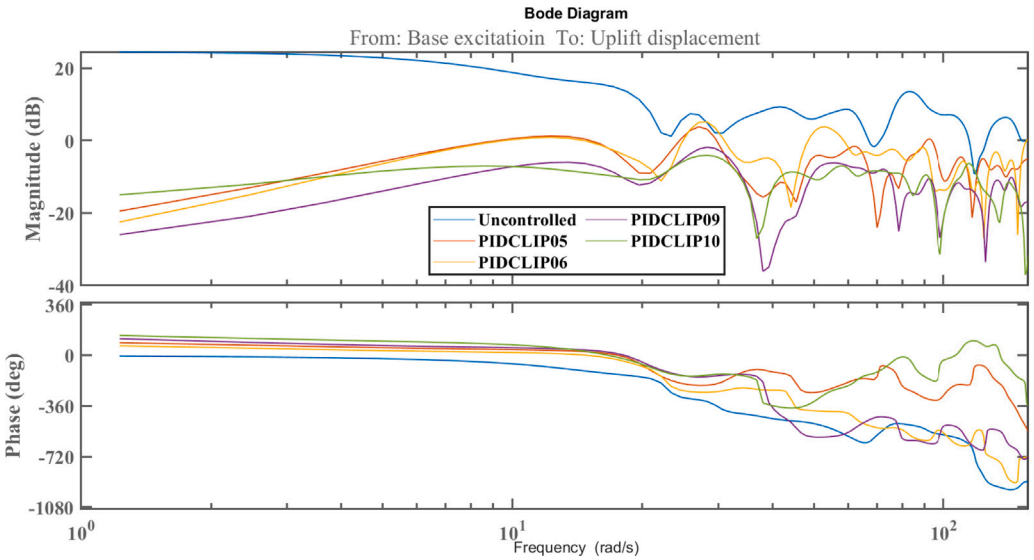

Fig. 16. Frequency response of the uncontrolled and controlled system using several semi-active controllers under the Christchurch 2011, 0.438 g, from input base excitation to the output uplift displacement of the tank at Channel No. 10 (LVDT02).

surpassed them in some cases. These controllers work only based on the online output measurements of the system in real-time, which act as the input to the control system design. More importantly, they are stable and robust to inaccuracies in mathematical representations of the system. Therefore, it is expected that they are scalable and applicable to any fluid-tank with different structural characteristics and geometrical shapes.

The non-parametric frequency responses of the uncontrolled and controlled system using different semi-active controllers from input base excitation to the output uplift of the tank were estimated by the Spectral Analysis (SPA) approach via the Blackman-Tukey method [109] using the Hann windowing. The non-parametric frequency response function using the Blackman-Tukey is obtained using the below function,

$$\hat{G}_N(e^{i\omega}) = \frac{\hat{\Phi}_{in/out}(\omega)}{\hat{\Phi}_{in}(\omega)} \tag{63}$$

where $\hat{\Phi}_{in}(\omega)$ and $\hat{\Phi}_{in/out}(\omega)$ are the Fourier transforms of the covariance and cross-covariance from input to output signals, respectively. These analyses were conducted using the System Identification toolbox of MATLAB R2023b to observe the effect of added control mechanism on the frequency behaviour of the system. The Bode diagram of the estimated frequency response of the uncontrolled and controlled system under Christchurch using different semi-active controllers has been depicted in Fig. 16.

Examining the magnitude plot in Fig. 16 for the uncontrolled system as well as the controlled system under a series of different controllers shows that the MR damper mechanism and the applied controllers have attenuated the structural responses of the system across a broad frequency range and improved its stability. Examining the phase plot in this figure demonstrates that the applied controllers have caused the system to exhibit less phase lag and improved the phase margin of the system. These results prove that the applied controllers are robust to both external disturbances and uncertainties in the dynamical representation of the system.

5. Conclusions

In this paper, numerical and experimental investigations were conducted to investigate the efficacy of MR dampers as smart semiactive control systems for rocking isolation and the development of seismic-resilient legged fluid tanks under based excitations. A series of equations were developed to model the dynamic behaviour of such complex structural systems. Numerical simulations and experimental tests under Near-Fault, Near-Fault Pulse-like, and Far-Fault earthquakes for the uncontrolled and controlled system were conducted using developed software platforms based on SIMULINK-MATLAB for data acquisition and control process. Four MR dampers were connected to the tank in a vertical configuration, one damper beside each leg, and tests using the developed control techniques were conducted to evaluate the performance of the controlled system and the control techniques in reducing the uplift displacement of such a tank as its most important structural response under earthquakes. The uplift displacement of the system was considered as the feedback to the control system design to achieve the control objective, being the minimisation of the uplift response of the fluid tank. Different passive, semi-active model-based, and data-driven adaptive control procedures were designed and tested for the fluid-tank-MR system.

Examining various passive and semi-active controllers applied to the experimentally tested fluid-tank-MR damper system demonstrated that, depending on the ground motion and the controller technique, the responses of the system can be reduced by different percentage points. The MR damper and the control strategies proved robust in the sense that even with inaccuracies, uncertainties, and model estimation errors in the mathematical representation of the considered complex system which entails fluid–structure interaction. Even in the case of the dampers operating as passive mechanisms, considerable reductions in the uplift displacement of the fluid tank are achievable. MR dampers are reliable control devices that do not rely on an external power supply, require very low voltage for operation, and convert to passive systems in the absence of the voltage and continue to mitigate the vibrations.

Comparisons between the experimental results and the theoretical uplift displacement of the tank based on the developed equations in this research demonstrated low modelling errors in the range of 6%–13% under the applied ground accelerations. After equipping the fluid-tank system with MR dampers, when the dampers operated as passive mechanisms, uplift displacement reductions up to 52% in the case of Passive Off (no voltage to the damper) and 83% in the case of Passive On (constant voltage of 3 V to the damper) were achieved. The model-based control techniques showed they could successfully attenuate responses up to considerable percentage points of up to 83%, depending on the applied ground motion and the controller. The designed data-driven techniques, by bridging the gap between the modelled dynamical system and the real structure, could adaptively

achieve the same level of performance as that of model-based techniques by relying only on input/output data in real time in spite of the available uncertainties and inaccuracies. According to the conducted experimental investigations, these techniques were able to mitigate the uplift response of the legged fluid tank up to 85%. Analysing the results of conducted numerical and experimental investigations in this research in both time and frequency domains proved the efficacy of the MR dampers and designed controllers for attenuating uplift displacements of legged rigid fluid tanks. Therefore, these devices can be considered as promising alternatives for providing flexible, fail-safe, robust, and reliable vertical connections and rocking isolators to protect fluid tanks against the destructive effects of base excitations. The low computational cost of the developed techniques and approaches makes them possible to be deployed on micro-controllers to develop autonomous control systems for developing fluid tanks that are resilient to base excitations in practical applications.

CRediT authorship contribution statement

Seyed Ehsan Aghakouchaki Hosseini: Writing – review & editing, Writing – original draft, Visualization, Validation, Software, Methodology, Investigation, Formal analysis, Data curation, Conceptualization. **Sherif Beskhyroun:** Writing – review & editing, Supervision, Resources, Project administration, Methodology, Funding acquisition, Conceptualization.

Declaration of competing interest

The authors declare that they have no known competing financial interests or personal relationships that could have appeared to influence the work reported in this paper.

Acknowledgements

Funding: This work was supported by the Natural Hazards Commission (Toka Tū Ake), Wellington, New Zealand [research grant No. 19/U780] within the Department of Built Environment Engineering, Faculty of Design and Creative Technologies, School of Future Environments, Auckland University of Technology (AUT), Auckland, New Zealand.

Appendix. Digital filters, transfer functions, and controllers

A.1. Digital filters

Low Pass Filter (LPF) transfer function over the RLS estimation parameters:

$$H_{LPF}(z) = \frac{0.0001}{z - 0.9999} \tag{A.1}$$

First-order filter over the voltage signal,

$$u(z) = \frac{0.6988}{z - 0.3012} \tag{A.2}$$

Low Pass Filter (LPF) over displacement measurements to estimate velocity:

Filter method: Recursive IIR digital filter
Filter order: 6
Passband edge frequency: 20 Hz
Maximum passband ripple: 0.1 dB
Minimum stopband attenuation: 80 dB

A.2. Model reference transfer functions

$$H_1(z) = \frac{0.0003943z + 0.0003937}{z^2 - 1.988z + 0.9953} \tag{A.3}$$

$$H_2(z) = \frac{2.187e-6z + 2.184e-6}{z^2 - 1.988z + 0.9953} \tag{A.4}$$

$$H_4(z) = \frac{2.469e-5z + 2.468e-5}{z^2 - 1.998z + 0.9988} \tag{A.5}$$

A.3. Model-based controllers and their parameters

PIDCLIP05: PID + Clipping algorithm,
Model transfer function: $H_1(z)$

$$Controller\ parameters: \begin{cases} K_P = 0.042862 \\ K_I = 1.3035 \\ K_D = 0 \\ N = 100 \end{cases} \tag{A.6}$$

PIDCLIP06: PID + Clipping algorithm,
Model transfer function: $H_2(z)$

$$Controller\ parameters: \begin{cases} K_P = 1.4169 \\ K_I = 141.6933 \\ K_D = 0 \\ N = 100 \end{cases} \tag{A.7}$$

PIDCLIP09: PID + Clipping algorithm,
Model transfer function: $H_4(z)$

$$Controller\ parameters: \begin{cases} K_P = 187.0527 \\ K_I = 421.0758 \\ K_D = 18.092 \\ N = 365.9331 \end{cases} \tag{A.8}$$

PIDCLIP10: PID + Clipping algorithm,
Model transfer function: $H_4(z)$

$$Controller\ parameters: \begin{cases} K_P = 731.9133 \\ K_I = 1161.545 \\ K_D = 55.7802 \\ N = 301.251 \end{cases} \tag{A.9}$$

PIDMCLIP03: PID + Modified Clipping algorithm,
Model reference transfer function: $H_4(z)$

$$Controller\ parameters: \begin{cases} K_P = 731.9133 \\ K_I = 1161.545 \\ K_D = 55.7802 \\ N = 301.251 \end{cases} \tag{A.10}$$

A.4. Data-driven adaptive controllers and their parameters

ODDAPIDC01: Online data-driven adaptive PID + Clipping algorithm, Model reference transfer function: $H_1(z)$
LPF transfer function: $H_{LPF}(z)$
ODDAPIDC06: Online data-driven adaptive PID + Clipping algorithm,
Model reference transfer function: $H_4(z)$
LPF transfer function: $H_{LPF}(z)$

$$Controller\ parameters\ for\ model\ reference: \begin{cases} K_P = 731.9133 \\ K_I = 1161.545 \\ K_D = 55.7802 \\ N = 301.251 \end{cases} \tag{A.11}$$

ODDAPIDMC01: Online data-driven adaptive PID + Modified Clipping algorithm,

Model reference transfer function: $H_4(z)$

LPF transfer function: $H_{LPF}(z)$

$$Controller\ parameters\ for\ model\ reference: \begin{cases} K_P = 187.0527 \\ K_I = 421.0758 \\ K_D = 18.092 \\ N = 365.9331 \end{cases} \quad (A.12)$$

ODDAPIDMC02: Online data-driven adaptive PID + Modified Clipping algorithm,

Model reference transfer function: $H_4(z)$

LPF transfer function: $H_{LPF}(z)$

$$Controller\ parameters\ for\ model\ reference: \begin{cases} K_P = 731.9133 \\ K_I = 1161.545 \\ K_D = 55.7802 \\ N = 301.251 \end{cases} \quad (A.13)$$

Data availability

Data will be made available on request.

References

[1] Zhai XWH, Feng F. Multi-physics coupling method and applications of fluid-structure interaction on LNG storage tanks. 2014.

[2] Calvi GM, Nascimbene R. Seismic design and analysis of tanks. John Wiley & Sons; 2023.

[3] Brunesi E, Nascimbene R, Pagani M, Beilic D. Seismic performance of storage steel tanks during the may 2012 emilia, Italy, earthquakes. J Perform Constr Facil 2015;29(5):04014137.

[4] Fischer EC, Liu J, Varma AH. Investigation of cylindrical steel tank damage at wineries during earthquakes : Lessons learned and mitigation opportunities. Pr Period Struct Des Constr 2016;21(3). http://dx.doi.org/10.1061/(ASCE)SC.1943-5576.0000283, 04016004–04016004.

[5] Yazdanian M, Ingham JM, Lomax W, Wood R, Dizhur D. Damage observations and remedial options for approximately 1500 legged and flat-based liquid storage tanks following the 2016 kaikōura earthquake. Structures 2020;24(February):357–76. http://dx.doi.org/10.1016/j.istruc.2020.01.024.

[6] Brunesi E, Nascimbene R. Effects of structural openings on the buckling strength of cylindrical shells. Adv Struct Eng 2018;21(16):2466–82.

[7] Brunesi E, Nascimbene R, Beilic D. Understanding the seismic resilience of metallic cylindrical tanks through parametric analysis.. Appl Sci (2076-3417) 2025;15(1).

[8] Shrimali MK, Jangid RS. A comparative study of performance of various isolation systems for liquid storage tanks. Int J Struct Stab Dyn 2002;2(04):573–91.

[9] Panchal V, Jangid R. Variable friction pendulum system for seismic isolation of liquid storage tanks. Nucl Eng Des 2008;238(6):1304–15.

[10] Panchal V, Jangid R. Behaviour of liquid storage tanks with VCFPS under near-fault ground motions. Struct Infrastruct Eng 2012;8(1):71–88.

[11] Moeindarbari H, Malekzadeh M, Taghikhany T. Probabilistic analysis of seismically isolated elevated liquid storage tank using multi-phase friction bearing. Earthquakes Struct 2014;6(1):111–25.

[12] Tsai C, Lin Y, Su H. Characterization and modeling of multiple friction pendulum isolation system with numerous sliding interfaces. Earthq Eng Struct Dyn 2010;39(13):1463–91.

[13] Gradinscak M, Semercigil S, Turan Ö. A sloshing absorber with a flexible container. 2011, p. 315–22.

[14] Oh S-H, Song S-H, Lee S-H, Kim H-J. Seismic response of base isolating systems with U-shaped hysteretic dampers. Int J Steel Struct 2012;12(2):285–98.

[15] Oh S-H, Song S-H, Lee S-H, Kim H-J. Experimental study of seismic performance of base-isolated frames with U-shaped hysteretic energy-dissipating devices. Eng Struct 2013;56:2014–27.

[16] Colombo JI, Almazán JL. Seismic reliability of continuously supported steel wine storage tanks retrofitted with energy dissipation devices. Eng Struct 2015;98:201–11. http://dx.doi.org/10.1016/j.engstruct.2015.04.037.

[17] Ormeño M, Geddes M, Larkin T, Chouw N. Experimental study of slip-friction connectors for controlling the maximum seismic demand on a liquid storage tank. Eng Struct 2015;103:134–46.

[18] Sahami K, Zarnani P, Quenneville P. Earthquake-resilience of storage tanks: using an innovative anchorage system. 2020, URL http://13.237.132.70/handle/nzsee/1710.

[19] Sahami K, Zarnani P, Quenneville P. Using a self-centring friction damper as anchorage system for industrial tanks and vessels. 2021, URL http://13.237.132.70/handle/nzsee/2381.

[20] De Angelis M, Giannini R, Paolacci F. Experimental investigation on the seismic response of a steel liquid storage tank equipped with floating roof by shaking table tests. Earthq Eng Struct Dyn 2010;39(4):377–96.

[21] Ozsarac V, Brunesi E, Nascimbene R. Earthquake-induced nonlinear sloshing response of above-ground steel tanks with damped or undamped floating roof. Soil Dyn Earthq Eng 2021;144:106673.

[22] Hasheminejad SM, Mohammadi MM. Active sloshing control in a smart flexible cylindrical floating roof tank. J Fluids Struct 2016;66:350–81. http://dx.doi.org/10.1016/j.jfluidstructs.2016.07.022.

[23] Hasheminejad SM, Mohammadi MM, Jamalpoor A. Hydroelastic modeling and active control of transient sloshing in a three dimensional rectangular floating roof tank. J Sound Vib 2020;470. http://dx.doi.org/10.1016/j.jsv.2019.115146, 115146–115146.

[24] Hernández E, Santamarina D. Active control of sloshing in containers with elastic baffle plates. Internat J Numer Methods Engrg 2012;91(6):604–21. http://dx.doi.org/10.1002/nme.4283, URL https://onlinelibrary.wiley.com/doi/abs/10.1002/nme.4283.

[25] Mehrvarz A, Najafi Ardekani A, Khodaei MJ, Jalili N. Vibration analysis and control of fluid containers using piezoelectrically-excited side wall. J Vib Control 2019;25(7):1393–408. http://dx.doi.org/10.1177/1077546318822374.

[26] Shrimali MK, Kasar AA. Seismic response of connected liquid tanks with MR dampers. In: 15th World Conference on Earthquake Engineering. Lisbon, Portugal; 2012.

[27] Hosseini SEA, Beskhyroun S. Fluid storage tanks: A review on dynamic behaviour modelling, seismic energy-dissipating devices, structural control, and structural health monitoring techniques. In: Structures. vol. 49, Elsevier; 2023, p. 537–56.

[28] Hosseini SEA, Beskhyroun S. Numerical investigations of seismic-resilient techniques for legged fluid storage tanks utilising magnetorheological dampers. In: Structures. vol. 68, Elsevier; 2024, 107090.

[29] Almazán JL, Cerda FA, Juan C, López-García D. Linear isolation of stainless steel legged thin-walled tanks. Eng Struct 2007;29(7):1596–611.

[30] Colombo J, Almazán J. Experimental investigation on the seismic isolation for a legged wine storage tank. J Constr Steel Res 2017;133:167–80.

[31] Reyes SI, Almazán JL, Vassiliou MF, Tapia NF, Colombo JI, de la Llera JC. Full-scale shaking table test and numerical modeling of a 3000-liter legged storage tank isolated with a vertical rocking isolation system. Earthq Eng Struct Dyn 2022;51(6):1563–85.

[32] Veletsos A. Seismic response and design of liquid storage tanks. Guid Seism Des Oil Gas Pipeline Syst 1984;255–370.

[33] Veletsos AS, Tang Y. Rocking response of liquid storage tanks. J Eng Mech 1987;113(11):1774–92. http://dx.doi.org/10.1061/(ASCE)0733-9399(1987)113:11(1774).

[34] Haroun MA, Ellaithy HM. Model for flexible tanks undergoing rocking. J Eng Mech 1985;111(2):143–57.

[35] Ishida K, Kobayashi N. An effective method of analyzing rocking motion for unanchored cylindrical tanks including uplift. 1988.

[36] Malhotra PK, Veletsos AS. Uplifting response of unanchored liquid-storage tanks. J Struct Eng 1994;120(12):3525–47. http://dx.doi.org/10.1061/(ASCE)0733-9445(1994)120:12(3525).

[37] Malhotra PK, Veletsos AS. Uplifting analysis of base plates in cylindrical tanks. J Struct Eng 1994;120(12):3489–505. http://dx.doi.org/10.1061/(ASCE)0733-9445(1994)120:12(3489).

[38] Malhotra PK, Veletsos AS. Beam model for base-uplifting analysis of cylindrical tanks. J Struct Eng 1994;120(12):3471–88. http://dx.doi.org/10.1061/(ASCE)0733-9445(1994)120:12(3471).

[39] Vathi M, Karamanos SA. Modeling of uplifting mechanism in unanchored liquid storage tanks subjected to seismic loading. 2014, p. 24–9, URL http://www.eaee.org/Media/Default/2ECCES/2ecces_ss/2385.pdf.

[40] Vathi M, Karamanos SA. Liquid storage tanks: Seismic analysis. In: Encyclopedia of earthquake engineering. Springer Berlin Heidelberg; 2014, p. 1–27. http://dx.doi.org/10.1007/978-3-642-36197-5_144-1.

[41] Vathi M, Karamanos SA. Simplified model for the seismic performance of unanchored liquid storage tanks. In: Pressure vessels and piping conference. 56987, American Society of Mechanical Engineers; 2015, V005T09A014. http://dx.doi.org/10.1115/PVP2015-45695.

[42] Vathi M, Karamanos SA. A simple and efficient model for seismic response and low-cycle fatigue assessment of uplifting liquid storage tanks. J Loss Prev Process Ind 2018;53:29–44. http://dx.doi.org/10.1016/j.jlp.2017.08.003.

[43] Housner GW. Earthquake pressures on fluid containers. In: 8th technical report under office of naval research. 1954.

[44] Haroun MA. Vibration studies and tests of liquid storage tanks. Earthq Eng Struct Dyn 1983;11(2):179–206.

[45] Haroun MA. Dynamic analyses of liquid storage tanks. 1980.

[46] Colombo J, Almazán J. Simplified 3D model for the uplift analysis of liquid storage tanks. Eng Struct 2019;196:109278.
[47] Ormeño M, Larkin T, Chouw N. Experimental study of the effect of a flexible base on the seismic response of a liquid storage tank. Thin-Walled Struct 2019;139:334–46.
[48] Ormeño M, Larkin T, Chouw N. Influence of uplift on liquid storage tanks during earthquakes. Coupled Syst Mech 2012;1(4):311–24.
[49] Ormeño M, Larkin T, Chouw N. The effect of seismic uplift on the shell stresses of liquid-storage tanks. Earthq Eng Struct Dyn 2015;44(12):1979–96.
[50] Housner GW. The behavior of inverted pendulum structures during earthquakes. Bull Seismol Soc Am 1963;53(2):403–17.
[51] Hogan S. The effect of damping on rigid block motion under harmonic forcing. Proc R Soc Lond Ser A: Mathematical Phys Sci 1992;437(1899):97–108.
[52] Vlachakis G, Giouvanidis AI, Mehrotra A, Lourenço PB. Numerical block-based simulation of rocking structures using a novel universal viscous damping model. J Eng Mech 2021;147(11):04021089.
[53] Casapulla C, Giresini L, Lourenço PB. Rocking and kinematic approaches for rigid block analysis of masonry walls: State of the art and recent developments. Build. 2017;7(3):69.
[54] Peña F, Prieto F, Lourenço PB, Campos Costa A, Lemos JV. On the dynamics of rocking motion of single rigid-block structures. Earthq Eng Struct Dyn 2007;36(15):2383–99.
[55] Dimitrakopoulos EG, DeJong MJ. Revisiting the rocking block: closed-form solutions and similarity laws. Proc R Soc A: Math Phys Eng Sci 2012;468(2144):2294–318.
[56] Zhang J, Makris N. Rocking response of free-standing blocks under cycloidal pulses. J Eng Mech 2001;127(5):473–83.
[57] Liu Y, Páez Chávez J, Brzeski P, Perlikowski P. Dynamical response of a rocking rigid block. Chaos: An Interdiscip J Nonlinear Sci 2021;31(7).
[58] Veletsos A. Seismic effects in flexible liquid storage tanks. In: Proceedings of the 5th world conference on earthquake engineering. vol. 1, Bulletin of the Seismological Society of America McLean, VA, USA; 1974, p. 630–9.
[59] Li Y, Hou Z. Data-driven asymptotic stabilization for discrete-time nonlinear systems. Systems Control Lett 2014;64:79–85.
[60] Bu X, Wang Q, Hou Z, Qian W. Data driven control for a class of nonlinear systems with output saturation. ISA Trans 2018;81:1–7.
[61] Asadi Y, Farsangi MM, Bijami E, Amani AM, Lee KY. Data-driven adaptive control of wide-area non-linear systems with input and output saturation: A power system application. Int J Electr Power Energy Syst 2021;133:107225.
[62] Markovsky I, Huang L, Dörfler F. Data-driven control based on the behavioral approach: From theory to applications in power systems. IEEE Control Syst Mag 2023;43(5):28–68.
[63] Hou Z-S, Wang Z. From model-based control to data-driven control: Survey, classification and perspective. Inform Sci 2013;235:3–35.
[64] Brunton SL, Noack BR. Closed-loop turbulence control: Progress and challenges. Appl Mech Rev 2015;67(5):050801.
[65] Tang W, Daoutidis P. Data-driven control: Overview and perspectives. In: 2022 American control conference. ACC, IEEE; 2022, p. 1048–64.
[66] Ziegler JG, Nichols NB. Optimum settings for automatic controllers. Trans Am Soc Mech Eng 1942;64(8):759–65.
[67] Madhekar SN, Jangid RS. Variable dampers for earthquake protection of benchmark highway bridges. Smart Mater Struct 2009;18(11):115011. http://dx.doi.org/10.1088/0964-1726/18/11/115011.
[68] Chen P-C, Tsai K-C, Lin P-Y. Real-time hybrid testing of a smart base isolation system. Earthq Eng Struct Dyn 2014;43(1):139–58.
[69] Prakash S, Jangid R. Seismic response of isolated structures with an improved model of the UFREI. In: Structures. vol. 42, Elsevier; 2022, p. 434–48.
[70] Naik KA, Gupta CP, Fernandez E. Design and implementation of interval type-2 fuzzy logic-PI based adaptive controller for DFIG based wind energy system. Int J Electr Power Energy Syst 2020;115:105468.
[71] Mohamed AA, Metwally H, El-Sayed A, Selem S. Predictive neural network based adaptive controller for grid-connected PV systems supplying pulse-load. Sol Energy 2019;193:139–47.
[72] Govindharaj A, Mariappan A. Real-time implementation of Chebyshev neural adaptive controller for boost converter. Int Trans Electr Energy Syst 2020;30(6):e12394.
[73] Öztürk S, Kahraman MF. Modeling and optimization of machining parameters during grinding of flat glass using response surface methodology and probabilistic uncertainty analysis based on Monte Carlo simulation. Meas 2019;145:274–91.
[74] Fan M, Wu G, Cao B, Sarkodie-Gyan T, Li Z, Tian G. Uncertainty metric in model-based eddy current inversion using the adaptive Monte Carlo method. Meas 2019;137:323–31.
[75] Fahmy RA, Badr RI, Rahman FA. Adaptive PID controller using RLS for SISO stable and unstable systems. Adv Power Electron 2014;2014(1):507142.
[76] Fahmy RA, Badr RI, Rahman FA. Alternative approach to use RLS algorithm in multivariable online adaptive PID controllers for MIMO systems. IETE J Res 2018;64(1):27–35.
[77] Al-Bargothi SN, Qaryouti GM, Jaber QM. Speed control of DC motor using conventional and adaptive pid controllers. Indones J Electr Eng Comput Sci 2019;16(3):1221–8.
[78] Ghamari SM, Mollaee H, Khavari F. Robust self-tuning regressive adaptive controller design for a DC–dc BUCK converter. Meas 2021;174:109071.
[79] Ibrahim RA. Liquid sloshing dynamics: theory and applications. Cambridge University Press; 2005.
[80] Spencer Jr B, Dyke S, Sain M, Carlson J. Phenomenological model for magnetorheological dampers. J Eng Mech 1997;123(3):230–8.
[81] Dominguez A, Sedaghati R, Stiharu I. Modeling and application of MR dampers in semi-adaptive structures. Comput Struct 2008;86(3–5):407–15.
[82] Mohebbi M, Dadkhah H, Rasouli Dabbagh H. Modified H2/LQG control algorithm for designing a multi-objective semi-active base isolation system. J Vib Control 2018;24(23):5693–704.
[83] Lavassani SHH, Shangapour S, Homami P, Gharehbaghi V, Farsangi EN, Yang T. An innovative methodology for hybrid vibration control (mr+ TMD) of buildings under seismic excitations. Soil Dyn Earthq Eng 2022;155:107175.
[84] Sreenivasappa B, Udaykumar R. Analysis and implementation of discrete time PID controllers using FPGA. Int J Electr Comput Eng 2010;2(1):71–82.
[85] Zand JP, Sabouri J, Katebi J, Nouri M. A new time-domain robust anti-windup PID control scheme for vibration suppression of building structure. Eng Struct 2021;244:112819.
[86] Dubey V, Goud H, Sharma PC. Role of PID control techniques in process control system: a review. Data Eng Smart Syst: Proc SSIC 2021 2022;659–70.
[87] Zhang H, Trott G, Paul R. Minimum delay PID control of interpolated joint trajectories of robot manipulators. IEEE Trans Ind Electron 1990;37(5):358–64.
[88] Shaban E, Sayed H, Abdelhamid A. A novel discrete pid+ controller applied to higher order/time delayed nonlinear systems with practical implementation. Int J Dyn Control 2019;7:888–900.
[89] Slate J, Sheppard L. Automatic control of blood pressure by drug infusion. IEE Proc A (Physical Sci Meas Instrum, Manag Educ Reviews) 1982;129(9):639–45.
[90] Marchetti G, Barolo M, Jovanovic L, Zisser H, Seborg DE. An improved PID switching control strategy for type 1 diabetes. Ieee Trans Biomed Eng 2008;55(3):857–65.
[91] Glickman S, Kulessky R, Nudelman G. Identification-based PID control tuning for power station processes. IEEE Trans Control Syst Technol 2004;12(1):123–32.
[92] Meng F, Liu S, Liu K. Design of an optimal fractional order PID for constant tension control system. IEEE Access 2020;8:58933–9.
[93] Şahin Ö, Adar NG, Kemerli M, Caglar N, Şahin İ, Parlak Z, Kükrek S, Engin T. A comparative evaluation of semi-active control algorithms for real-time seismic protection of buildings via magnetorheological fluid dampers. J Build Eng 2021;42:102795.
[94] Jansen LM, Dyke SJ. Semiactive control strategies for MR dampers: comparative study. J Eng Mech 2000;126(8):795–803.
[95] Zhang Y, Xu W, Du D, Wang S. Stochastic optimization of dissipation structures based on Lyapunov differential equations and the full stress design method. Build 2023;13(3):665.
[96] Goodwin GC, Sin KS. Adaptive filtering prediction and control. Courier Corporation; 2014.
[97] Mansour T. PID control: implementation and tuning. BoD–Books on Demand; 2011.
[98] Solvang PS. State Space Model Based PID Controller Tuning. (Master's thesis), University of South-Eastern Norway; 2019.
[99] Dyke SJ, Spencer Jr. B, Sain M, Carlson J. Modeling and control of magnetorheological dampers for seismic response reduction. Smart Mater Struct 1996;5(5):565.
[100] Kamalzare M, Johnson EA, Wojtkiewicz SF. Computationally efficient design of optimal strategies for controllable damping devices. Struct Control Heal Monit 2015;22(1):1–18.
[101] Abdeddaim M, Djerouni S, Ounis A, Athamnia B, Farsangi EN. Optimal design of magnetorheological damper for seismic response reduction of base-isolated structures considering soil-structure interaction. In: Structures. vol. 38, Elsevier; 2022, p. 733–52.
[102] Yoshida O, Dyke SJ. Seismic control of a nonlinear benchmark building using smart dampers. J Eng Mech 2004;130(4):386–92.
[103] Pohoryles DA, Duffour P. Adaptive control of structures under dynamic excitation using magnetorheological dampers: an improved clipped-optimal control algorithm. J Vib Control 2015;21(13):2569–82.
[104] Pei P, Peng Y, Qiu C. An improved semi-active structural control combining optimized fuzzy controller with inverse modeling technique of MR damper. Struct Multidiscip Optim 2022;65(9):272.
[105] Brandão FDS, Miguel LFF. A new methodology for optimal design of hybrid vibration control systems (mr+ TMD) for buildings under seismic excitation. Shock Vib 2023;2023(1):8159716.
[106] Gao X. Development of a robust framework for real-time hybrid simulation: from dynamical system, motion control to experimental error verification (Ph.D. thesis), Purdue University; 2012.
[107] Ancheta TD, Darragh RB, Stewart JP, Seyhan E, Silva WJ, Chiou BS-J, Wooddell KE, Graves RW, Kottke AR, Boore DM, et al. NGA-West2 database. Earthq Spectra 2014;30(3):989–1005.
[108] Seismosoft. SeismoSignal – signal processing of strong-motion data. 2022, [accessed 20 June 2022] URL https://seismosoft.com/products/seismosignal/.
[109] Ljung L. System identification. In: Signal analysis and prediction. Springer; 1998, p. 163–73.